Int. J. Electrochem. Sci., 8 **(2013)** 5961 - 5979

International Journal of
ELECTROCHEMICAL
SCIENCE
www.electrochemsci.org

Computational and Experimental Evaluation of the Acid Corrosion Inhibition of Carbon Steel by 7-Methyl-2 Phenylimidazo[1,2-α]Pyridine

A. Anejjar [1], *A. Zarrouk* [2], *R. Salghi* [1,*], *D. Ben Hmamou* [1], *H. Zarrok* [3], *S. S. Al-Deyab* [4], *M. Bouachrine* [5], *B. Hammouti* [2], *N. Benchat* [2]

[1] Laboratory of Environmental Engineering and Biotechnology, ENSA, University Ibn Zohr, PO Box 1136, 80000 Agadir, Morocco
[2] LCAE-URAC 18, Faculty of Science, University of Mohammed Premier, Po Box 717 60000 Oujda, Morocco
[3] Laboratory separation processes, Faculty of Science, University Ibn Tofail PO Box 242, Kenitra, Morocco.
[4] Petrochemical Research Chair, Chemistry Department, College of Science, King Saud University, P.O. Box 2455, Riyadh 11451, Saudi Arabia.
[5] ESTM, Université Moualy Ismail, Meknes, Morocco.
[*]E-mail: r_salghi@yahoo.fr

Received: 28 January 2013 / *Accepted:* 9 March 2013 / *Published:* 1 April 2013

A newly synthesized 7-methyl-2-phenylimidazo[1,2-α]pyridine (MPP), was investigated as corrosion inhibitor of carbon steel in 1.0 M HCl solution using weight loss measurements, polarization and electrochemical impedance spectroscopy (EIS) methods. Results obtained revealed that MPP is effective corrosion inhibitor for carbon steel in hydrochloric acid and its efficiency attains more than 93.7% at 298 K. The adsorption of pyridine derivative is found to obey Langmuir adsorption isotherm, and the thermodynamic parameters were determined and discussed. The relationship between molecular structure of this compound and their inhibition efficiency has been investigated by quantum chemical calculations. The electronic properties such as the highest occupied molecular orbital (HOMO), the lowest unoccupied molecular orbital (LUMO) energy levels, energy gap (LUMO-HOMO), dipole moment and molecular orbital densities were computed.

Keywords: Pyridine derivative, Steel, Corrosion inhibition, Polarization curves, EIS.

1. INTRODUCTION

Acid solutions are widely used in industry, the most important fields of application being acid pickling, industrial cleaning, acid descaling, oil-well acidizing and petrochemical processes [1-

3].However, most of acid media cause the detriment of materials and considerable economic losses [4]. To overcome this unavoidable problem, inhibitors are generally used. The study of material corrosion processes and their inhibition by organic inhibitors is a very active field of research [5-27]. However, the efficiency of these inhibitors depends on the nature and the state of the metallic surfaces, chemical composition, and structure of the inhibitor. Furthermore, the stability of the adsorbed inhibitor films formed over the metal surface to protect the metal from corrosion depends on some physico-chemical properties of the molecule, related to its functional groups, aromaticity, the possible steric effects, electronic density of donors, type of corrosive medium and nature of the interaction between the inhibitor and the metal surface [28-30]. This interaction is generally explained by the formation of an adsorptive film of a physical and/or chemical character on the metal surface. Adsorption of inhibitors may block either cathodic, anodic, or both reactions. The electrostatic attraction between the charged inhibitor molecules and the charge-active centers on the metal surface leads to physisorption. Data in the literature show that most organic inhibitors adsorb on metals by displacing water molecules on the surface and forming a compact barrier film [30-32]. One of the most effective ways to judge whether the nature of interaction is Physisorption or chemisorption is to calculate the thermodynamic parameters for the adsorption process.

The inhibiting performance of this inhibitor was evaluated by weight loss, polarization curves, and EIS. Also the relationship between quantum chemical calculations and experimental inhibition efficiencies of the inhibitor was discussed. The chemical structure of the studied MPP derivative is given in Fig 1.

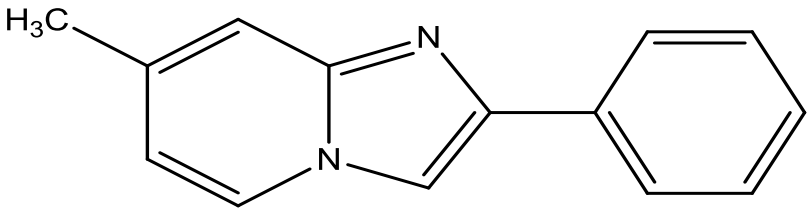

Figure 1. 7-Methyl-2-Phenylimidazo[1,2-α]Pyridine (MPP).

2. EXPERIMENTAL METHODS

2.1. Materials

The steel used in this study is a carbon steel (Euronorm: C35E carbon steel and US specification: SAE 1035) with a chemical composition (in wt%) of 0.370 % C, 0.230 % Si, 0.680 % Mn, 0.016 % S, 0.077 % Cr, 0.011 % Ti, 0.059 % Ni, 0.009 % Co, 0.160 % Cu and the remainder iron (Fe). The carbon steel samples were pre-treated prior to the experiments by grinding with emery paper SiC (120, 600 and 1200); rinsed with distilled water, degreased in acetone in an ultrasonic bath immersion for 5 min, washed again with bidistilled water and then dried at room temperature before use. The acid solutions (1.0 M HCl) were prepared by dilution of an analytical reagent grade 37 % HCl with double-distilled water. The concentration range of 7-methyl-2-phenylimidazo[1,2-α]pyridine (MPP) employed was 10^{-6} M to 10^{-3} M.

2.2. Measurements

2.2.1. Weight loss measurements

The gravimetric measurements were carried out at definite time interval of 6 h at room temperature using an analytical balance (precision ± 0.1 mg). The carbon steel specimens used have a rectangular form (length = 1.6 cm, width = 1.6 cm, thickness = 0.07 cm). Gravimetric experiments were carried out in a double glass cell equipped with a thermostated cooling condenser containing 80 mL of non-de-aerated test solution. After immersion period, the steel specimens were withdrawn, carefully rinsed with bidistilled water, ultrasonic cleaning in acetone, dried at room temperature and then weighted. Triplicate experiments were performed in each case and the mean value of the weight loss was calculated.

2.2.2. Electrochemical measurements

Electrochemical experiments were conducted using impedance equipment (Tacussel-Radiometer PGZ 100) and controlled with Tacussel corrosion analysis software model Voltamaster 4. A conventional three-electrode cylindrical Pyrex glass cell was used. The temperature is thermostatically controlled. The working electrode was carbon steel with the surface area of 1 cm^2. A saturated calomel electrode (SCE) was used as a reference. All potentials were given with reference to this electrode. The counter electrode was a platinum plate of surface area of 1 cm^2. A saturated calomel electrode (SCE) was used as the reference; a platinum electrode was used as the counter-electrode. All potentials are reported *vs*. SCE. All electrochemical tests have been performed in aerated solutions at 298 K.

For polarization curves, the working electrode was immersed in a test solution during 30 min until a steady state open circuit potential (E_{ocp}) was obtained. The polarization curve was recorded by polarization from -800 to -400 mV/SCE with a scan rate of 1 mV s^{-1}. AC impedance measurements were carried-out in the frequency range of 100 kHz to 10 mHz, with 10 points per decade, at the rest potential, after 30 min of acid immersion, by applying 10 mV ac voltage peak-to-peak. Nyquist plots were made from these experiments. The best semicircle can be fit through the data points in the Nyquist plot using a non-linear least square fit so as to give the intersections with the *x*-axis.

2.4. Quantum chemical calculations

All theoretical calculations were performed using DFT (density functional theory) with the Beck's three parameter exchange functional along with the Lee-Yang-Parr nonlocal correlation functional (B3LYP) [33-35] with 6- 31G* basis set is implemented in Gaussian 03 program package [36]. This approach is shown to yield favorable geometries for a wide variety of systems. The following quantum chemical parameters were calculated from the obtained optimized molecular structure: the energy of the highest occupied molecular orbital (E_{HOMO}), the energy of the lowest unoccupied molecular orbital (E_{LUMO}), the energy band gap ($\Delta E_{gap} = E_{HOMO} - E_{LUMO}$), the dipole moment ($\mu$), the electron affinity (A), the ionization potential (I) and the number of transferred electrons (ΔN).

3. RESULTS AND DISCUSSION

3.1. Electrochemical experiment

3.1.1. Polarization curves

Fig. 2 shows polarization curves of the working electrode in 1.0 M HCl in the presence and absence of pyridine derivative. From Fig. 2 we can get the corrosion current density (I_{corr}) bextrapolating the Tafel lines to the corrosion potential [37]. The corrosion inhibition efficiency, η_{Tafel} %, was calculated by the equation:

$$\eta_{Tafel}\% = \frac{I^{\circ}_{corr} - I^{i}_{corr}}{I^{\circ}_{corr}} \times 100 \quad (1)$$

where, I°_{corr} and I^{i}_{corr} are the corrosion current density in absence and presence of inhibitor, respectively.

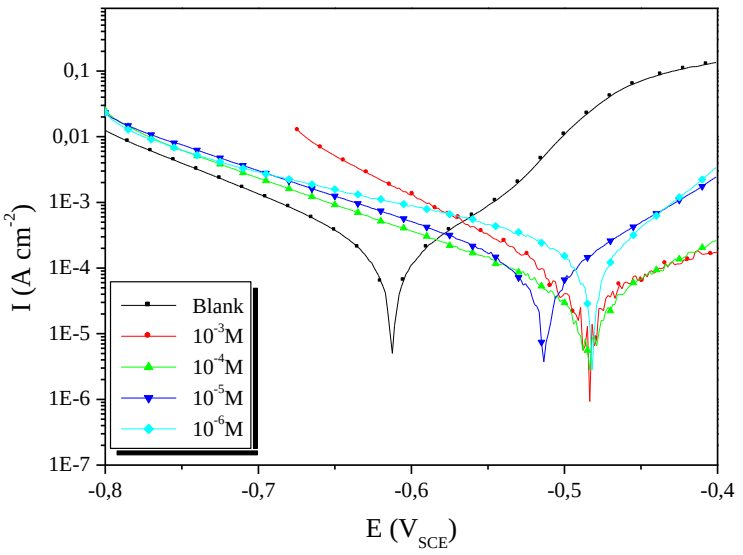

Figure 2. Potentiodynamic polarisation curves of carbon steel in 1.0 M HCl in the presence of different concentrations of MPP.

The complete electrochemical parameters E_{corr}, I_{corr} and cathodic Tafel slope (β_c), inhibition efficiency are calculated by polarization measurements and listed in Table 1. In hydrochloric acid solution the following mechanism is proposed for the corrosion of iron [38].

The anodic dissolution mechanism of iron is:

$$Fe + Cl^{-} \Leftrightarrow (FeCl^{-})_{ads} \quad (2)$$

$$(FeCl^{-})_{ads} \Leftrightarrow (FeCl)_{ads} + e^{-} \quad (3)$$

$$(FeCl)_{ads} \rightarrow (FeCl^{+})_{ads} + e^{-} \quad (4)$$

$$(FeCl^{+}) \Leftrightarrow Fe^{2+} + Cl^{-} \quad (5)$$

The cathodic hydrogen evolution mechanism is:

$$Fe + H^{+} \Leftrightarrow (FeH^{+})_{ads} \quad (6)$$

$$(FeH^{+})_{ads} + e^{-} \rightarrow (FeH)_{ads} \quad (7)$$

$$(FeH)_{ads} + H^{+} + e^{-} \rightarrow Fe + H_2 \quad (8)$$

The parallel cathodic Tafel curves in Fig. 2 suggest that the hydrogen evolution is activation-controlled and the reduction mechanism is not affected by the presence of the inhibitor. The values of β_c changed with increasing inhibitor concentration, which indicates the influence of the compound on the kinetics of hydrogen evolution.

Table 1 show that the addition of any of the studied pyridine derivative in the concentration range 10^{-6} to 10^{-3}M reduces significantly the dissolution rate of carbon steel. The efficiency is increased as the inhibitor concentration is increased. The corrosion potential E_{corr}, shifted towards more anodic values in the presence of this compound. The shift of E_{corr} with increasing of the inhibitor concentration due to the fact that the inhibitor has a strong influence on the iron dissolution. E_{corr} values was shifted towards less negative (noble) potential which is a necessary to quote the inhibitive action of inhibitor and to classify an inhibitor into an anodic, a cathodic, or mixed type. It has been reported that [39], an inhibitor can be classified as an anodic or a cathodic-type inhibitor on the basis of magnitude of shift in Ecorr value. If displacement in E_{corr} is greater than 85 mV, towards anode or cathode with reference to blank, then an inhibitor is categorized as either anodic or cathodic type inhibitor, respectively. Otherwise an inhibitor is treated as mixed type. In our study, minimum displacement in E_{corr} value was around 100 mV indicating pyridine derivative is a anodic type inhibitor.

Table 1. Electrochemical parameters of carbon steel at various concentrations of MPP in 1.0 M of HCl and corresponding inhibition efficiency.

Inhibitor	Conc (M)	$-E_{corr}$ (mV/SCE)	$-\beta_c$ (mV dec^{-1})	I_{corr} ($\mu A\ cm^{-2}$)	η_{Tafel} (%)
Blank	1.0	612	110	231	-
MPP	1×10^{-3}	482	16	115	93.1
	1×10^{-4}	484	34	117	85.3
	1×10^{-5}	512	60	129	74.0
	1×10^{-6}	483	97	130	58.0

3.1.2. The electrochemical impedance spectroscopy (EIS)

3.1.2.1. Effect of concentration inhibitor

Nyquist plots of pyridine compound in 1.0 M HCl solutions in the absence and presence of various concentrations of MPP are given in Fig. 3. The impedance spectra show a single semicircle

and the diameter of semicircle increases with increasing inhibitor concentration. These diagrams exhibit that the impedance spectra consist of one capacitive loop at high frequency, the high frequency capacitive loop was attributed to charge transfer of the corrosion process [40]. Then, it is noticed that the impedance spectra show a "depressed" semicircle at the center under the real axis, such phenomenon often refer to the frequency dispersion of interfacial impedance which has been attributed to the roughness; inhomogeneity of the solid surfaces and adsorption of inhibitor [41,42]. The impedance of the inhibited steel increases with increasing the inhibitor's concentration and consequently the inhibition efficiency increases. The equivalent circuit compatible with the Nyquist diagram recorded in the presence of inhibitors was depicted in Fig. 4.

The simplest approach requires the theoretical transfer function $Z(\omega)$ to be represented by a parallel combination of a resistance R_{ct} and a capacitance C, both in series with another resistance R_s [43]:

$$Z(\omega) = R_s + \frac{1}{1/R_{ct} + i\omega C} \quad (9)$$

ω is the frequency in rad/s, $\omega = 2\pi f$ and f is frequency in Hz. To obtain a satisfactory impedance simulation of carbon steel, it is necessary to replace the capacitor (C) with a constant phase element (CPE) Q in the equivalent circuit. The most widely accepted explanation for the presence of CPE behavior and depressed semicircles on solid electrodes is microscopic roughness, causing an inhomogeneous distribution in the solution resistance as well as in the double-layer capacitance [44]. Constant phase element CPE_{dl}, R_s and R_{ct} can be corresponded to double layer capacitance, solution resistance, and charge transfer resistance respectively. To corroborate the equivalent circuit, the experimental data are fitted to equivalent circuit and the circuit elements are obtained. Table 2 illustrates the equivalent circuit parameters for the impedance spectra of corrosion of carbon steel in 1.0 M HCl solution. The results demonstrate that the presence of inhibitor enhance the value of R_{ct} obtained in the pure medium while that of Q_{dl} is reduced. The decrease in Q_{dl} values was caused by adsorption of inhibitor indicating that the exposed area decreased. On the other hand, a decrease in Q_{dl}, which can result from a decrease in local dielectric constant and/or an increase in the thickness of the electrical double layer, suggests that pyridine derivative inhibitor act by adsorption at the metal-solution interface.

According to the equivalent circuit, the impedance data were fitted and the electrochemical parameters were given in Table 2, the inhibition efficiency η_z% in various concentrations of MPP is calculated by charge transfer resistance as followed [45]:

$$\eta_z\% = \frac{R_{ct(inh)} - R_{ct}}{R_{ct(inh)}} \times 100 \quad (10)$$

where R_{ct} and $R_{ct\ (inh)}$ were the values of polarization resistance in the absence and presence of inhibitor, respectively.

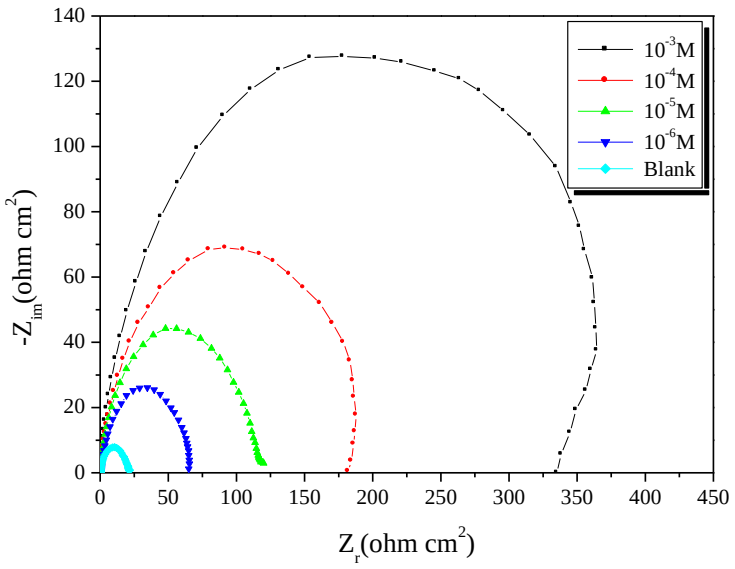

Figure. 3. Nyquist diagrams for carbon steel electrode with and without MPP at E_{corr} after 30 min of immersion.

Table 2. Electrochemical Impedance parameters for corrosion of carbon steel in acid medium at various contents concentrations of MPP.

Conc (M)	R_s (Ω cm^2)	R_{ct} (Ω cm^2)	Q_{dl} (μF cm^{-2})	η_z (%)
Blank	1.7	21	160.37	-----
1×10^{-3}	1.6	335	40.45	93.7
1×10^{-4}	1.5	182	45.24	88.5
1×10^{-5}	1.7	120	47.16	82.5
1×10^{-6}	1.8	65	75.06	67.7

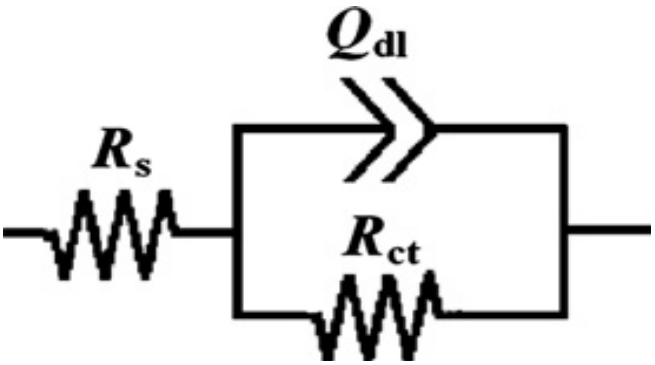

Figure 4. Equivalent circuits compatible with the experimental impedance data in Fig.3.

As it can be seen from Table 2, the increase in values of R_{ct} and the decrease in values of Q_{dl} with increasing the concentration also indicate that pyridine derivative act as primary interface inhibitor and the charge transfer controls the corrosion of carbon steel under the open circuit conditions.

3.1.2.2. Effect of temperature

Temperature plays an important role on the progress of the corrosion reactions of carbon steel in HCl solutions. Increasing the temperature increases the energy of the reactants to form the activated complex which dissociates to yield the corrosion products [46]. The effect of temperature on the inhibition efficiencies of MPP was also studied by EIS in the temperature range 298-328K (Figs. 5 and 6).

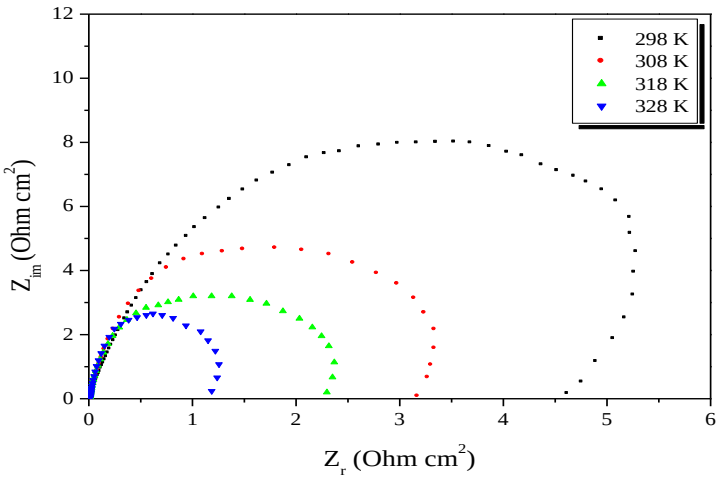

Figure 5. Nyquist diagrams for carbon steel in 1.0 M HCl at different temperatures.

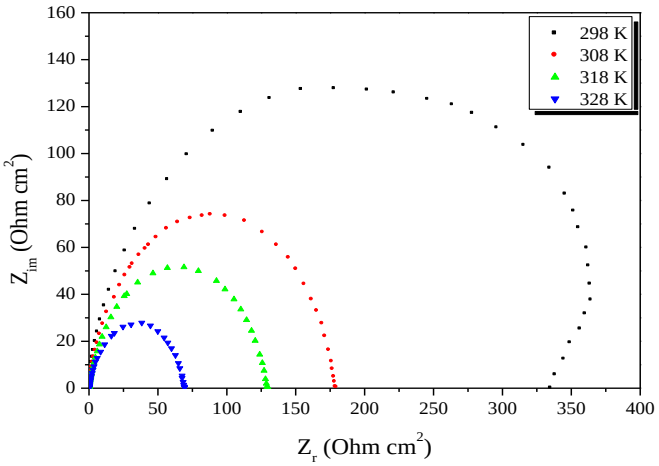

Figure 6. Nyquist diagrams for carbon steel in 1 M HCl + 10^{-3}M of MPP at different Temperatures.

As the corrosion rate is inversely proportional to R_{ct} values of Ln ($1/R_{ct}$) and Ln($1/R_{ct}$)/T were plotted as a function of temperature (Arrhenius plots) in Figs. 7 and 8 for the corrosion of carbon steel in hydrochloric acid solutions. Values of E_a and ΔH_a and ΔS_a were estimated from the slopes of the straight lines and given in Table 3.

Table 3. Thermodynamic parameters for the adsorption of MPP in 1.0 M HCl on the carbon steel at different temperatures.

Inhibitor	T (K)	R_{ct} (Ω cm^2)	C_{dl} (μF cm^{-2})	η_z (%)
Blank	298	21	85.31	----
	308	13	80.41	----
	318	10	65.13	----
	328	5.4	50.09	----
MPP	298	335	23.76	93.7
	308	179	35.58	92.7
	318	129	30.86	92.2
	328	69	36.63	92.2

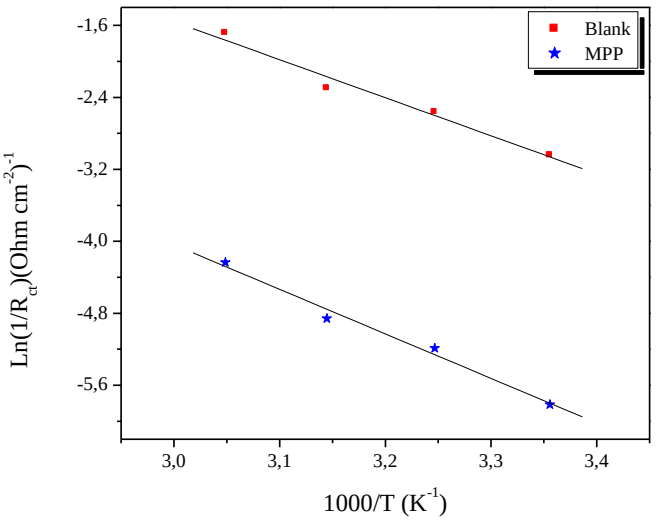

Figure 7. Arrhenius plots of carbon steel in 1.0 M HCl with and without 10^{-3}M of MPP.

Table 4. The value of activation parameters for carbon steel in 1.0 M HCl in the absence and presence of 10^{-3}M of MPP.

Inhibitor	E_a (kJ/mol)	ΔH_a (kJ/mol)	ΔS_a (J/mol K)	$E_a - \Delta H_a$ (KJ/mol)
Blank	35.14	32.54	-161.04	2.60
MPP	41.14	48.54	-163.64	2.60

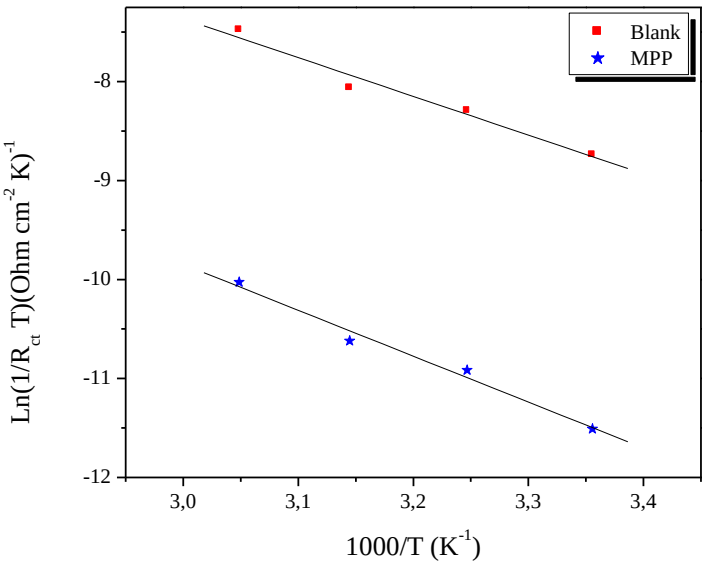

Figure 8. Arrhenius plots of carbon steel in 1.0 M HCl with and without 10^{-3}M of MPP.

Inspection of Table 4 shows that the value of E_a determined in solutions containing MPP is higher than that of in the absence of inhibitor (blank). The increase in E_a in the presence of this inhibitor may be interpreted as physical adsorption that occurs in the first stage [47]. Szauer and Brand explained that the increase in activation energy can be attributed to an appreciable decrease in the adsorption of the inhibitor on the carbon steel surface with increase in temperature. A corresponding increase in the corrosion rate occurs because of the greater area of metal that is consequently exposed to the acid environment [48]. The positive sign of the enthalpie ΔH_a reflect the endothermic nature of the steel dissolution process and mean that the dissolution of steel is difficult [49]. We remark that E_a and ΔH_a values vary in the same way (Table 4). This result permit to verify the known thermodynamic reaction between the E_a and ΔH_a as shown in Table 4 [50]:

$$\Delta H_a = E_a - RT \qquad (11)$$

ΔS_a increases negatively with the presence of MPP than the uninhibited; this reflects the formation of an ordered stable layer of inhibitor on the steel surface [51].

3.2. Gravimetric study

The values of percentage inhibition efficiency (η_{WL}) obtained from weight loss experiment for the corrosion of carbon steel in 1.0 M HCl in the presence of different concentration of pyridine compound at different temperature are given in Table 5. The η_{WL} was calculated from the following relationship:

$$\eta_{WL}\% = \frac{w^{\circ} - w}{w^{\circ}} \times 100 \qquad (12)$$

where w° and w are weight loss in the absence and presence of inhibitor.
The rate of corrosion ρ (g cm^{-2} h^{-1}) was calculated from equation:

$$\rho = \frac{w^{\circ} - w}{St} \qquad (13)$$

where S is surface area of steel plate and t is immersion time.

Table 5. Corrosion parameters obtained from weight loss measurements for carbon steel in 1.0 M HCl containing various concentration of inhibitor at 298 K.

Inhibitor	Conc (M)	ρ (mg cm^{-2} h^{-1})	η_{WL} (%)	θ
Blank	1.0	1.001	-----	-----
MPP	1×10^{-3}	0.073	92.7	0.927
	1×10^{-4}	0.139	86.1	0.861
	1×10^{-5}	0.216	78.4	0.784
	1×10^{-6}	0.390	61.0	0.610

The variation of η_{WL} with the concentration of inhibitor, at 298K is shown in Fig. 9 which revealed that pyridine derivative has got significant inhibition ability, in 1.0 M HCl media. The data in Table 5 indicates the η_{WL} increased with the increase in inhibitor concentration. The increase of η_{WL} with inhibitor concentration primarily indicates that the magnitude of adsorption and surface coverage by inhibitor molecules on the surface of steel increases with inhibitor concentration [52].

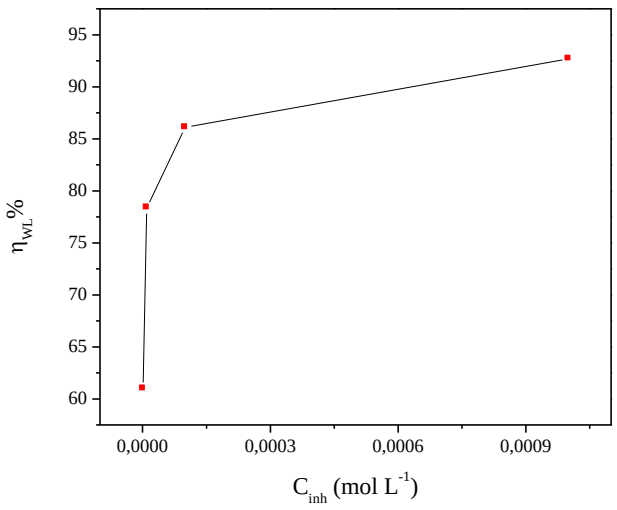

Figure 9. The variation of η_{WL} with inhibitor concentration at 298K.

3.3. Adsorption and thermodynamic considerations

Basic information on the interaction between the organic compounds and metal surfaces can be provided from the adsorption isotherms. The values of surface coverage, θ, corresponding to different concentrations of inhibitors at 298K have been used to explain the best isotherm to determine the adsorption isotherm. The adsorption isotherms generally considered were [53]:

Temkin isotherm

$$\exp(f.\theta) = K_{ads}.C_{inh} \quad (14)$$

Langmuir isotherm

$$\frac{\theta}{1-\theta} = K_{ads}.C_{inh} \quad (15)$$

Frumkin isotherm

$$\frac{\theta}{1-\theta}.\exp(-2f.\theta) = K_{ads}.C_{inh} \quad (16)$$

Freundluich isotherm

$$\theta = K_{ads}.C_{inh} \quad (17)$$

where K_{ads} is the equilibrium constant of the inhibitor adsorption process, C_{inh} the inhibitor concentration and f is the factor of energetic inhomogeneity, the surface coverage (θ) can obtain from weight loss measurements, it calculated by the following equation [54]:

$$\theta = \frac{w^{\circ} - w}{w^{\circ}} \quad (18)$$

For MPP, the plot of C_{inh}/θ versus C_{inh} yielded straight line with slope value of 1.07. This slope is close to 1, and the strong correlation ($R^2 > 0.99998$) proved that the adsorption of MPP on the metal surface obeyed to the Langmuir's adsorption isotherm (Fig. 10).

According to the Langmuir isotherm [55], K_{ads} values can be calculated from the intercepts of the straight lines on the C_{inh}/θ- axis, the K_{ads} is related to the standard free energy of adsorption, ΔG°_{ads}, with the following equation:

$$\Delta G^{\circ}_{ads} = -RTLn(55.5K_{ads}) \quad (19)$$

The value 55.5 in the above equation is the molar concentration of water in solution in mol/L [56]. Thermodynamic parameters for adsorption process obtained from Langmuir's adsorption isotherm for the studied inhibitors are given in Table 6.

As it can be seen from Table 6, the addition of inhibitor causes negative values of ΔG°_{ads}, it indicated that adsorption of studied compound is spontaneous process [57]. It generally accepted that the values of ΔG°_{ads} up to -20 kJ mol^{-1}, the types of adsorption were regarded as physisorption, the inhibition acts due to the electrostatic interactions between the charged molecules and the charged metal, while the values around -40 kJ mol^{-1} or smaller, were seen as chemisorption, which is due to the charge sharing or a transfer from the inhibitor molecules to the metal surface to form a covalent bond [58,59].

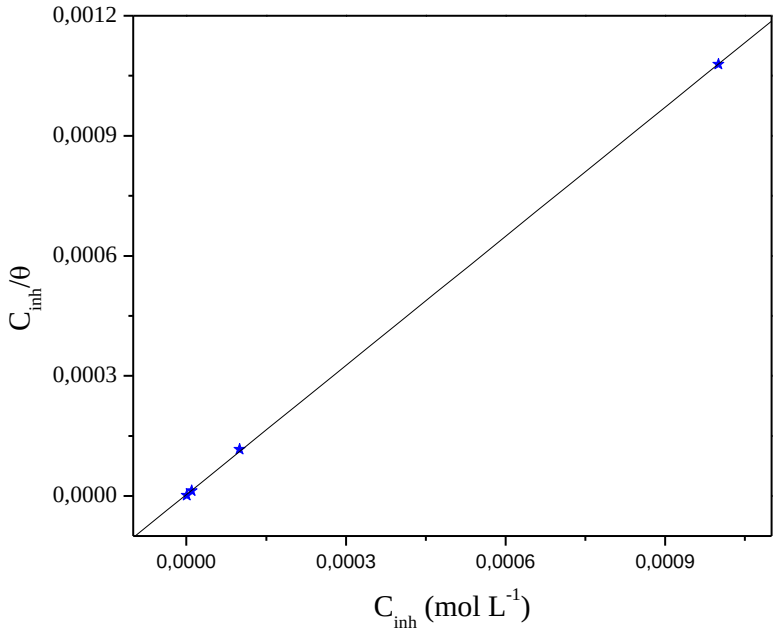

Figure 10. Langmuir adsorption of MPP on the carbon steel surface in 1.0 HCl solution.

Table 6. Thermodynamic parameters for the adsorption of MPP in 1.0 M HCl on the carbon steel at 298K.

Inhibitor	Slope	K_{ads} (M^{-1})	R^2	ΔG°_{ads} (kJ/mol)
MPP	1.07	281587.02	0.99998	-41.04

The values of ΔG°_{ads} in our measurements is -41.04 kJ mol^{-1} (in Table 6), it is suggested that the adsorption of this compound involves two types of interaction, chemisorption more than physisorption.

3.4. Quantum chemical calculations

Theoretical chemistry has been used recently to explain the mechanism of corrosion inhibition, such as quantum chemical calculations [60,61]. Quantum chemical calculations have been proven to be a very powerful tool for studying the mechanism [62,63]. The objective of this work is to present the relationships between the pyridine derivative reactivity and their ability to inhibit the corrosion of carbon steel in hydrochloric acid. The structural parameters, such as the the energy of the highest occupied molecular orbital (E_{HOMO}), the energy of the lowest unoccupied molecular orbital (E_{LUMO}), the energy band gap ($\Delta E_{gap} = E_{HOMO} - E_{LUMO}$), the dipole moment ($\mu$), the electron affinity (A), the ionization potential (I) and the fraction of electrons (ΔN) transfer from inhibitor to iron were calculated and correlated with inhibition efficiencies.

The effectiveness of an inhibitor is related to its spatial molecular structure as well as with its molecular electronic structure [64]. In this regard, quantum chemical calculations have proved to be a powerful tool for studying corrosion inhibition mechanism and recently, corrosion publications have contained substantial quantum chemical calculations [65,66]. In this study, quantum chemical calculations were conducted by the density functional theory (DFT) level with the 3-21G(d) basis sets by geometry optimization of the studied compound in order to support experimental data and to investigate the relationship between molecular structure of the pyridine derivative and their inhibition effects. Fig. 11 represents the optimized structure of pyridine derivative.

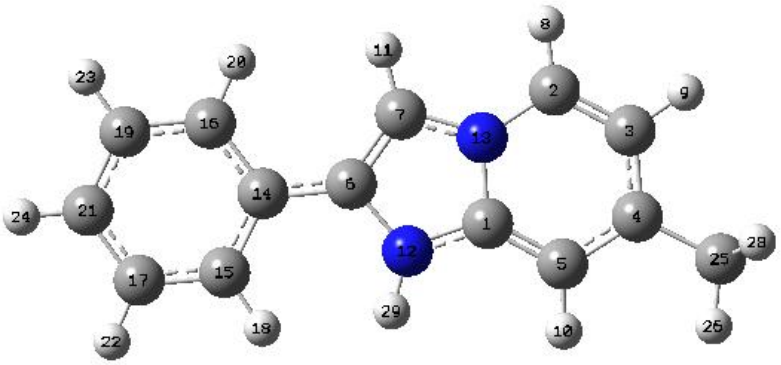

Figure 11. Optimized molecular structure of MPP by B3LYP-6-31G(d) method.

The HOMO and LUMO populations of the studied pyridine derivative are shown in Fig. 12. It can be seen in Fig. 12, that both HOMO and LUMO are distributed throughout the molecule.

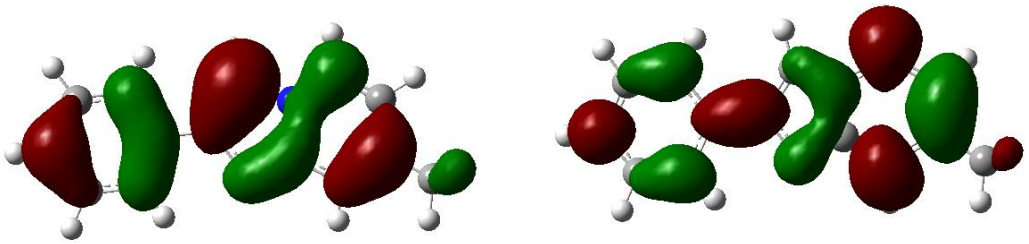

HOMO **LUMO**

Figure 12. The frontier molecular orbital density distributions of MPP.

The use of Mulliken population analyses to probe adsorption centers of inhibitors has been widely reported [67-70]. There is a general consensus by several researchers that the more negatively charged a heteroatom is, the more it can be adsorbed on the metal surface through the donor-acceptor type reaction [71-73]. It has also been reported that electrophiles attack molecules at sites of negative charge [74], which means that from the values of Mulliken charges in Table 7, it is possible to assume that all the nitrogen atoms present a considerable excess of negative charge -0.58 and -0.49 and negative charges around most carbon atoms of the aromatic rings, in the neutral and protonated forms, this suggest that the most probable reactive site for the adsorption of iron is located on the nitrogen atoms.

Table 7. Mulliken charge density data of MPP.

MPP	**MPP$^+$**
C1 0.558891	C1 0.643633
C2 0.073731	C2 0.009363
C3 -0.228602	C3 -0.214611
C4 0.187745	C4 0.165187
C5 -0.245785	C5 -0.278432
C6 0.173666	C6 0.241673
C7 -0.025758	C7 -0.035503
N12 -0.585228	N12 -0.791047
N13 -0.489506	N13 -0.499970
C14 0.101300	C14 0.136770
C15 -0.171674	C15 -0.196031
C16 -0.177991	C16 -0.180984
C17 -0.132847	C17 -0.128572
C19 -0.138915	C19 -0.137205
C21 -0.126139	C21 -0.140652
C25 -0.530272	C25 -0.529025

The electronic parameters give information about the tendency of the inhibitor to interact with the metal surface, and such an ability of an inhibitor lies largely in its electronic distribution. The electronic distribution of molecules is understood by investigating their frontier molecular orbital's and the electron density parameters, such as the dipole moment and the partial atomic charges. The frontier molecular orbital's are the highest occupied molecular orbital (HOMO) and the lowest unoccupied molecular orbital (LUMO) for a given molecule. The quantum chemical parameters necessary for a meaningful discussion of the current work are reported in Table 8 and include the energy of the HOMO (E_{HOMO}), the energy of the LUMO (E_{LUMO}), the HOMO-LUMO energy difference (E_{H-L}), the dipole moment (μ), the ionization potential (I), etc.

The results for the calculations of the ionization potential (I) and the electron affinity (A) by application of the Koopmans' theorem [75] are shown in Table 8. According to the Hartree-Fock theorem, the frontier orbital energies are given by: $I = -E_{HOMO}$; $A = -E_{LUMO}$. This theorem establishes a relation between the energies of the HOMO and the LUMO and the ionization potential and the electron affinity, respectively. Although no formal proof of this theorem exists within DFT, its validity is generally accepted. For χ and η, their operational and approximate definitions are $\chi = \frac{I + A}{2}$,

$\eta = \frac{I - A}{2}$. Two systems, Fe and inhibitor, are brought together, electrons will flow from lower χ (inhibitor) to higher χ (Fe), until the chemical potentials become equal. As a first approximation, the fraction of electrons transferred [76], ΔN, will be given by:

$$\Delta N = \frac{\chi_{Fe} - \chi_{inh}}{2\left(\eta_{Fe} + \eta_{inh}\right)}$$

where Fe is the Lewis acid according to HSAB theory [77]. The difference in electronegativity drives the electron transfer, and the sum of the hardness parameters acts as a resistance [76]. In order to calculate the fraction of electrons transferred, a theoretical value for the electronegativity of bulk iron was used $\chi_{Fe} \approx 7$eV [75], and a global hardness of $\eta_{Fe} \approx 0$, by assuming that for a metallic bulk I=A [78] because they are softer than the neutral metallic atoms.

Table 8. Some molecular properties of MPP calculated using DFT at the B3LYP/6-31G (d) basis set in aqueous phase both in neutral and protonated form.

Molecular parameters	MPP	MPP^+
μ (Debye)	3.4303	0.7884
E_{HOMO} (eV)	-5.449	-2.4221
E_{LUMO} (eV)	-0.9471	-0.4697
ΔE_{gap} (eV)	4.5018	1.9523
I (eV)	5.449	2.4221
A (eV)	0.9471	0.4697
χ (eV)	3.19805	1.4459
η (eV)	2.25095	0.9762
ΔN (eV)	0.844521	2.844755

A comparison of the calculated molecular descriptors across structures of the protonated specie and nonprotonated specie provides information on the variation of the trends in the molecular properties due to protonation effect. The results, reported in Table 8, show that, E_{HOMO} is much higher in the protonated specie than in the nonprotonated specie, which implies that the protonated specie is better electron donors than the nonprotonated specie; the highest dipole moment (3.43 D) in the nonprotonated specie, indicating a strong tendency of the molecule to donate electrons to appropriate acceptor molecules of low empty molecular orbital energy of the metal and increasing adsorption between MPP and metal surface; E_{LUMO} is much higher in the protonated specie than in the nonprotonated specie; the calculations in Table 8 further show that MPP in the protonated form (MPP^+) has the smallest ΔE value (1.95 eV) indicating that MPP^+ is the most reactive inhibitor that can easily adsorb on themetal surface causing higher protection, the number of electrons transferred is higher in the protonated specie than in the nonprotonated spice. In all cases, the value of $\Delta N < 3.6$, agrees with the study initially proposed by Lukovit and reported elsewhere that inhibition efficiency

increased with increasing electron donating ability at the metal surface [79]. All these factors indicate that the nonprotonated species has the higher tendency to donate electrons to the metal surface.

4. CONCLUSIONS

7-methyl-2-phenylimidazo[1,2-α]pyridine (MPP) is found to be good inhibitors for carbon steel corrosion in 1.0 M HCl. The inhibition is accomplished by adsorption of MPP molecules on the iron surface, and the adsorption is spontaneous and obeys the Langmuir isotherm. The inhibition efficiency of MPP increases with the increase in the inhibitor concentration and decreases with the increase in temperature of the corrosion medium. Energy of activation for the corrosion process increases in the presence of inhibitor. MPP acts as a cathodic type inhibitor. Data obtained from quantum chemical calculations using DFT at the B3LYP/6-31G (d) level of theory were correlated to the inhibitive effect of pyridine derivative. Both experimental and theoretical calculations are in excellent agreement.

ACKNOWLEDGEMENTS
Prof S. S. Al-Deyab and Prof B. Hammouti extend their appreciation to the Deanship of Scientific Research at king Saud University for funding the work through the research group project.

References

1. F. Bentiss, M. Largenee, M. Tralsnel, *J. Appl. Electroch*. 29 (1999) 1073.
2. T.Y. Soror, H.A. El-Dahan, N.G. El-Sayed Ammer, *J. Mater. Sci. Technol*. 15 (1999) 16.
3. H.B. Fan, C.Y. Fu, H.L. Wang, X.P. Guo, J.S. Zheng, *Br. Corros. J*. 37 (2002) 122.
4. Y. Dud, R. Govea-Rueda, M. Galicia, *J. Phys. Chem*. B 109 (2005) 2674.
5. A. K. Singh, M. A. Quraishi, *J. Mater. Environ. Sci.* 1 (2) (2010) 101.
6. D.D.N. Singh, T.B. Singh, B. Gaur, *Corros. Sci*. 37 (1995) 1005.
7. M. Prajila, J. Sam, J. Bincy, J. Abraham, *J. Mater. Environ. Sci.* 3 (6) (2012) 1045.
8. U.J. Naik, V.A. Panchal, A.S. Patel, N.K. Shah, *J. Mater. Environ. Sci.* 3 (5) (2012) 935.
9. A. Zarrouk, H. Zarrok, R. Salghi, B. Hammouti, F. Bentiss, R. Touir, M. Bouachrine, *J. Mater. Environ. Sci.* 4 (2013) 177.
10. H. Zarrok, H. Oudda, A. Zarrouk, R. Salghi, B. Hammouti, M. Bouachrine , *Der Pharm. Chem*. 3 (2011) 576.
11. H. Zarrok, R. Salghi, A. Zarrouk, B. Hammouti, H. Oudda, Lh. Bazzi, L. Bammou, S. S. Al-Deyab, *Der Pharm. Chem*. 4 (2012) 407.
12. H. Zarrok, S. S. Al-Deyab, A. Zarrouk, R. Salghi, B. Hammouti, H. Oudda, M. Bouachrine, F. Bentiss, *Int. J. Electrochem. Sci*. 7 (2012) 4047.
13. D. Ben Hmamou, R. Salghi, A. Zarrouk, H. Zarrok, B. Hammouti, S. S. Al-Deyab, M. Bouachrine, A. Chakir, M. Zougagh, *Int. J. Electrochem. Sci*. 7 (2012) 5716.
14. A. Zarrouk, B. Hammouti, S.S. Al-Deyab, R. Salghi, H. Zarrok, C. Jama, F. Bentiss, *Int. J. Electrochem. Sci*. 7 (2012) 5997.
15. A. Zarrouk, H. Zarrok, R. Salghi, B. Hammouti, S.S. Al-Deyab, R. Touzani, M. Bouachrine, I. Warad, T. B. Hadda, *Int. J. Electrochem. Sci*. 7 (2012) 6353.
16. A. Zarrouk, M. Messali, H. Zarrok, R. Salghi, A. Al-Sheikh Ali,B. Hammouti, S. S. Al-Deyab, F. Bentiss, *Int. J. Electrochem. Sci*. 7 (2012) 6998.

17. H. Zarrok, A. Zarrouk, R. Salghi, Y. Ramli, B. Hammouti, S. S. Al-Deyab, E. M. Essassi, H. Oudda, *Int. J. Electrochem. Sci*. 7 (2012) 8958.
18. D. Ben Hmamou, R. Salghi, A. Zarrouk, H. Zarrok, S. S. Al-Deyab, O. Benali, B. Hammouti, *Int. J. Electrochem. Sci.* 7 (2012) 8988.
19. A. Zarrouk, M. Messali, M. R. Aouad, M. Assouag, H. Zarrok, R. Salghi, B. Hammouti, A. Chetouani, *J. Chem. Pharm. Res*. 4 (2012) 3427.
20. D. Ben Hmamou, M. R. Aouad, R. Salghi, A. Zarrouk, M. Assouag, O. Benali, M. Messali, H. Zarrok, B. Hammouti, *J. Chem. Pharm. Res*. 4 (2012) 3489.
21. H. Zarrok, H. Oudda, A. El Midaoui, A. Zarrouk, B. Hammouti, M. Ebn Touhami, A. Attayibat, S. Radi, R. Touzani, Res. Chem. Intermed (2012) DOI 10.1007/s11164-012-0525-x
22. A. Zarrouk, B. Hammouti, H. Zarrok, R. Salghi, A. Dafali, Lh. Bazzi, L. Bammou, S. S. Al-Deyab, *Der Pharm. Chem*. 4 (2012) 337
23. A. Zarrouk, A. Dafali, B. Hammouti, H. Zarrok, S. Boukhris, M. Zertoubi, *Int. J. Electrochem. Sci*. 5 (2010) 46.
24. A. Zarrouk, T. Chelfi, A. Dafali, B. Hammouti, S.S. Al-Deyab, I. Warad, N. Benchat, M. Zertoubi, *Int. J. Electrochem. Sci*. 5 (2010) 696.
25. A. Zarrouk, I. Warad, B. Hammouti, A. Dafali, S.S. Al-Deyab, N. Benchat, *Int. J. Electrochem. Sci*. 5 (2010) 1516.
26. A. Zarrouk, B. Hammouti, R. Touzani, S.S. Al-Deyab, M. Zertoubi, A. Dafali, S. Elkadiri, *Int. J. Electrochem*. Sci. 6 (2011) 4939.
27. A. Zarrouk, B. Hammouti, H. Zarrok, S.S. Al-Deyab, M. Messali, *Int. J. Electrochem. Sci*. 6 (2011) 6261.
28. V.S. Sastry, Corrosion Inhibitors. Principles and Applications, JohnWiley& Sons, New York, 1998.
29. F. Bentiss, M. Lagrenee, M. Traisnel, *Corrosion*, 56 (2000) 733.
30. F. Bentiss, M. Traisnel, M. Lagrene´e, *J. Appl. Electrochem*. 31 (2001) 41.
31. L.G. Qiu, A.J. Xie, Y.H. Shen, *Corros. Sci*. 47 (2005) 273.
32. A. Ghazoui, R. Saddik, N. Benchat, B. Hammouti, M. Guenbour, A. Zarrouk, M. Ramdani , *Der Pharma Chim.* 4 (2012) 352.
33. A.D. Becke. *J. Chem. Phys*. 96 (1992) 9489.
34. A.D. Becke. *J. Chem. Phys*., 98 (1993) 1372.
35. C. Lee, W. Yang, R.G. Parr. *Phys. Rev. B*. 37 (1988) 785.
36. Gaussian 03, Revision B.01, M. J. Frisch, et al., Gaussian, Inc., Pittsburgh, PA, (2003).
37. K.F. Khaled, N. Hackerman, *Electrochim. Acta*, 48 (2003) 2715.
38. A. Yurta, A. Balaban b, S. Ust¨un Kandemir, *Mater. Chem. Phys*. 85 (2004) 420.
39. Ishtiaque Ahamad, Rajendra Prasad, M.A. Quraishi, *Corros. Sci*. 52 (2010) 1472.
40. H. Ashassi-Sorkhabi, N. Ghalebsaz-Jeddi, F. Hashemzadeh, H. Jahani, *Electrochim. Acta*, 51 (2006) 3848.
41. T. Paskossy, *J. Electroanal. Chem*. 364 (1994) 111.
42. F.B. Growcock, J.H. Jasinski, *J. Electrochem. Soc*. 136 (1989) 2310.
43. I. Danaee, *J. Electroanal. Chem*. 662 (2011) 415.
44. I. Danaee, S. Noori, *Int. J. Hydrogen Energy*, 36 (2011) 12102.
45. H. Zarrok, A. Zarrouk, B. Hammouti, R. Salghi, C. Jama, F. Bentiss, *Corros. Sci*. 64 (2012) 243.
46. N.A. Negm, A.M. El Sabagh, M.A. Migahed, H.M. Abdel Bary, H.M. El Din, *Corros. Sci*. 52 (2010) 2122.
47. E.F. El Sherbini, *Mater. Chem. Phys*. 60 (1999) 286.
48. T. Szauer, A. Brand, *Electrochim. Acta*, 26 (1981) 1219.
49. N.M. Guan, L. Xueming, L. Fei, *Mater. Chem. Phys*. 86 (2004) 59.
50. M.K. Gomma, M.H. Wahdan, *Mater. Chem. Phys*. 39 (1995) 209.
51. A. Yurt, A. Balaban, S.U. Kandemir, G. Bereket, B. Erk, *Mater. Chem. Phys*. 85 (2004) 420.

52. Ashish Kumar Singh, M.A. Quraishi, *Corros. Sci*. 52 (2010) 152.
53. D. Do, Adsorption Analysis: Equilibria and Kinetics, Imperial College Press, 1980.
54. B. Hammouti, A. Zarrouk, S.S. Al-Deyab And I. Warad, *Orient. J. Chem.*, 27 (2011) 23.
55. R. Agrawal, T.K.G. Namboodhiri, *Corros. Sci*. 30 (1990) 37.
56. J. Flis, T. Zakroczymski, *J. Electrochem. Soc*. 143 (1996) 2458.
57. I. El Ouali B. Hammouti, A. Aouniti, Y. Ramli, M. Azougagh, E.M. Essassi, M. Bouachrine, *J.Mater. Environ. Sci.* 1 (2010) 1
58. S. Hari Kumar, S. Karthikeyan, *J. Mater. Environ. Sci.* 3 (2012) 925
59. A. Zarrouk, H. Zarrok, R. Salghi, B. Hammouti, F. Bentiss, R. Touir, M. Bouachrine, *J. Mater. Environ. Sci*. 4 (2013) 177
60. A. Stoyanova, G. Petkova, S.D. Peyerimhoff, *Chem. Phys*. 279 (2002) 1.
61. A.Y. Musa, A.A.H. Kadhum, A.B. Mohamad, A.A.B. Rahoma, H. Mesmari, *J. Mol. Struct*. 969 (2010) 233.
62. L.T. Sein Jr., A.L. Cederberg-Crossley, *J. Mol. Struct*. 1004 (2011) 319.
63. N.O. Obi-Egbedi, I.B. Obot, M.I. El-Khaiary, *J. Mol. Struct*. 1002 (2011) 86.
64. I.B. Obot, N.O. Obi-Egbedi, S.A. Umoren, *Corros. Sci*. 51 (2009) 276.
65. I.B. Obot, N.O. Obi-Egbedi, *Colloids Surf. A* 330 (2008) 207.
66. G. Gece, *Corros. Sci*. 50 (2008) 2981.
67. J. Fang, J. Li, *J. Mol. Struct*. 593 (2002) 171.
68. B. Hasanov, M. Sadikoglu, S. Bilgic, *Appl. Surf. Sci*. 253 (2007) 3913.
69. N.K. Allam, *Appl. Surf. Sci*. 253 (2007) 4570.
70. F. Kandemirli, S. Sagdina, *Corros. Sci*. 49 (2007) 2118.
71. G. Bereket, C. Ogretir, C. Ozsahim, *J. Mol. Struct*. 663 (2003) 39.
72. M. Ozcan, I. Dehri, M. Erbil, *Appl. Surf. Sci*. 236 (2004) 155.
73. W. Li, Q. He, C. Pei, B. Hou, *Electrochim. Acta*, 52 (2007) 6386.
74. M. Ozcan, I. Dehri, M. Erbil, *Prog. Org. Coat.* 51 (2004) 181.
75. V.S. Sastri, J.R. Perumareddi, *Corros. Sci*. 53 (1997) 617.
76. R.G. Pearson, *Inorg. Chem*. 27 (1988) 734.
77. R.G. Pearson, *J. Am. Chem. Soc*. 85 (1963) 3533.
78. M.J.S. Dewar, W. Thiel, *J. Am. Chem. Soc*. 99 (1977) 4899.
79. I. Lukovits, E. Lalman, F. Zucchi, *Corrosion*, 57 (2001) 3.